GENERAL YIELD CONDITIONS IN A PLASTICITY ANALYSIS OF SOIL-WHEEL INTERACTION

E. Nowatzki, et al

Grumman Aerospace Corporation
Bethpage, New York

December 1972

RM-563J

GENERAL YIELD CONDITIONS IN A PLASTICITY ANALYSIS OF SOIL-WHEEL INTERACTION

December 1972

RESEARCH DEPARTMENT

GRUMMAN AEROSPACE CORPORATION
BETHPAGE NEW YORK

U

Security Classification

DOCUMENT CONTROL DATA - R & D

(Security classification of title, body of abstract and indexing annotation must be entered when the overall report is classified)

1. ORIGINATING ACTIVITY (Corporate author)	2a. REPORT SECURITY CLASSIFICATION
Grumman Aerospace Corporation	U
	2b. GROUP

3. REPORT TITLE

General Yield Conditions in a Plasticity Analysis of Soil-Wheel Interaction

4. DESCRIPTIVE NOTES (Type of report and inclusive dates)

Research Report

5. AUTHOR(S) (First name, middle initial, last name)

E. Nowatzki and L. Karafiath

6. REPORT DATE	7a. TOTAL NO. OF PAGES	7b. NO. OF REFS
December 1972	36	21

8a. CONTRACT OR GRANT NO.	9a. ORIGINATOR'S REPORT NUMBER(S)
b. PROJECT NO.	RM-563J
c. N/A	9b. OTHER REPORT NO(S) (Any other numbers that may be assigned this report)
d.	N/A

10. DISTRIBUTION STATEMENT

Approved for public release; distribution unlimited.

11. SUPPLEMENTARY NOTES	12. SPONSORING MILITARY ACTIVITY

13. ABSTRACT

Plasticity theory and a general representation of the Mohr failure criterion are applied to the problem of soil-wheel interaction. Load, drawbar pull (or drag), torque are computed for a rigid wheel being driven on sand obtained from Jones Beach, Long Island, New York. Analytical results obtained from soutions using a conventional Mohr-Coulcomb linear failure envelope are compared to those obtained from a nonlinear solution. Conclusions are drawn from the comparison that attest the importance of considering the nonlinearity of failure envelopes in certain cases for accuracy of soil-wheel interaction prediction. Preliminary experimental results show reasonable agreement with predicted values of wheel performance parameters.

DD FORM 1 NOV 68 1473

U

Security Classification

Grumman Research Department Memorandum RM-563J

GENERAL YIELD CONDITIONS IN A PLASTICITY ANALYSIS OF SOIL-WHEEL INTERACTION†

by

E. Nowatzki and L. Karafiath

Materials and Structural Mechanics

December 1972

†Presented at the 8th U.S. National Off-Road Mobility Symposium, West Lafayette, Indiana, October 1972.

Approved by: Charles E. Mack, Jr.
Charles E. Mack, Jr.
Director of Research

TABLE OF CONTENTS

LIST OF ILLUSTRATIONS

INTRODUCTION

In recent years, plasticity theory has been applied successfully to a number of problems involving soil-strength and soil-structure interaction (Refs. 1-5). In most of the analyses, a Mohr-Coulomb yield criterion is used that postulates a linear relationship between the two principal stresses in the plane of deformation. Hill (Ref. 6), Sokolovskii (Ref. 1), and Szymanski (Ref. 7) have set up the equations of plastic equilibrium to include general nonlinear yield conditions. Kingston and Spencer (Ref. 8), in applying these equations to the problem of the indentation of a semi-infinite mass of material by a flat, smooth rigid punch, have suggested that the numerical computation can be effected without too much difficulty and with a relatively small increase in computing time.

SCOPE

In this paper, the differential equations of plastic equilibrium obtained from plasticity theory and a general yield condition are applied to the problem of the interaction between soil and a driven rigid wheel. A computer program, written in general terms, is used to compute values of load, drawbar pull, and torque for specified soil parameters and wheel sizes. Results obtained from solutions, using a conventional straight line Mohr-Coulomb failure criterion, are compared to those in which a curved failure envelope was used for an 8-inch-diameter, 2-inch-wide rigid wheel being driven on Jones Beach sand. The soil parameters for this soil were determined in previous studies and were used as research tools to compare theory with experimental results. This comparison shows that the theory is well suited for natural soils having a nonlinear envelope. Partially saturated soils and certain types of soils with specific loading histories, e.g., overconsolidated clays, show failure envelopes that are significantly curved. In these cases, consideration of this nonlinearity is essential for the accuracy of wheel-soil interaction prediction.

FAILURE CONDITIONS IN SOIL BENEATH WHEELS

Observations of soil deformations beneath driven or towed rigid wheels suggest that the soil fails in two distinct zones (Refs. 9,10). The zones are forward and to the rear of the point at which the maximum normal stress occurs along the soil-wheel interface. The reaction of the soil in the forward failure zone resists the motion of the wheel, while the reaction of the backward zone actually enhances it by providing a forward acting component. Under certain conditions, single zone failure occurs; however, this is not the usual case and it will not be considered here.

Although evidence of failure in the third dimension exists (Refs. 11,12), the forward and rear failure zones are assumed to form only in the radial plane of the wheel. The state of stress at a specific point on the soil-wheel interface is shown diagrammatically in Fig. 1a. The Mohr-Coulomb yield criterion was chosen to express the limiting relationship between shear and normal stresses. Figure 1b shows the Mohr circle of stress (Circle I) for the stress conditions at the point on the interface depicted in Fig. 1a. Other circles (II and III) can be constructed for different stress states at other points along the interface or in the soil mass. The illustration also shows how the major and minor principal stresses, their respective directions, and the directions of the i- and j-characteristic slip lines are obtained from the Mohr diagram for the stress condition at the specific point on the interface. When these quantities are transferred back to Fig. 1a, the directions of the principal stresses relative to the stresses at that point on the soil-wheel interface are clearly seen.

The stress envelope (linear or nonlinear) shown in Fig. 1b is defined by an equation in which the soil strength parameters c (cohesion) and φ (angle of internal friction) relate shear stress to normal stress at failure. The nonlinear envelope represents the curve that is tangent to the three Mohr stress circles shown. The straight line usually used to approximate the curvilinear failure envelope can introduce errors at the lower stress levels. The failure envelope for effective stresses is defined in general terms by the equation

$$\left(\frac{\tau}{d}\right)^m - \frac{\sigma_n}{k} - c = 0 \qquad (1)$$

where

τ = shear stress at failure

σ_n = effective normal stress (as defined in Ref. 13) at failure

c = cohesion

m, d, k = constants that define the curvature of the failure envelope.

For the linear case ($d = m = 1$ and $k = \cot \varphi$) Eq. (1) reduces to the more conventional Mohr-Coulomb form used widely in soil mechanics (Ref. 14):

$$\tau = \sigma_n \tan \varphi + c \qquad (2)$$

where φ = angle of internal friction of the soil.

In the analysis of the interaction between a rigid wheel and soil, all stresses along the soil-wheel interface and throughout the soil mass are assumed to act in planes parallel to the radial plane of the wheel. The magnitude, direction, and distribution of

stresses beneath a rigid wheel are functions of the strength parameters (c, φ, γ) of the supporting soil and certain properties of the wheel [geometry, coefficient of friction (tan δ) between wheel material and soil, mode of propulsion]. In wheel-performance studies, relationships are established among the so-called "performance parameters" — load, torque, and drawbar pull (or drag). The summation of the vertical components of the normal and shear stresses along the soil-wheel interface perimeter and across the wheel width equals the load; similarly, the summation of the components parallel to the surface is a measure of the drawbar pull. The torque is determined from the magnitude and distribution of the shear stresses.

The application of this method of wheel performance analysis is strictly valid only in cases where soil inertia forces can be neglected and where the soil strength parameters are referred to effective stresses. Inasmuch as the kinematics of the problem are not considered in the analysis, the results must be a lower bound solution. Experiments performed at Grumman and elsewhere have shown that in loose, frictional soils, the actual failure conditions correspond quite closely to those implied by the lower bound solution (Ref. 14).

THE NATURE OF THE FAILURE ENVELOPE

The results of triaxial compression tests on air-dried Jones Beach sand are shown in Fig. 2. The origin (0,0) must be considered a data point for the failure envelope of this material because this sand is not cohesive in an air-dried condition. Even without this constraint, a straight line cannot be drawn tangent to all the circles. Two limiting straight line envelopes are shown, one at an angle (φ) of 41 degrees for the low stress levels, the other at 36 degrees for the higher stress levels. An "average" straight line envelope (not shown) would tend to underestimate the strength of the material at low stress levels and overestimate it at high stress levels. Because it diverges from the correct strength envelope at the higher stress levels, the "average" straight line becomes a progressively worse approximation. A nonlinear envelope corresponding to Eq. (1) is also shown in Fig. 2. It is clear from the figure that it provides a good approximation to the Mohr circles at all stress levels.

The implications of using the nonlinear envelope in the solution of the differential equations of plasticity and the associated stress distributions beneath rigid wheels is best shown with reference to Fig. 3. In Fig. 3a, two Mohr circles, A and B, corresponding to the nonlinear failure envelope are shown together with a $\varphi = 41°$ envelope, a linear envelope corresponding to Circle A for a cohesionless material. In plasticity theory, normal stresses are related to the intersection of the failure envelope with the σ axis. In the case of a cohesionless material, this intersection coincides with the origin of the $\tau - \sigma$ coordinate system. For the same material, the use of a nonlinear envelope results in a ψ intercept on the σ axis (refer to Fig. 3b).

Even though the Mohr circle for the stresses at points A and D in Figs. 3b and 3d, respectively, is the same for both the linear and nonlinear failure envelope (Circle A), the shear and normal stresses developed at the interface, assuming the same angle of interface friction (δ), are different in the two cases (refer to points a and d in Figs. 3a and 3c, respectively). Since shear stresses at the interface are the major contributors to drawbar pull, the importance of using a nonlinear envelope for the soil-wheel interaction problems is evident.

FORMULATION FOR A DRIVEN RIGID WHEEL

The following set of differential equations represents a theoretically rigorous formulation to the general two dimensional problem of determining the plastic stress states and slip line fields in a soil mass due to loading conditions on specified boundaries of the soil mass:

$$dz = dx \tan(\theta \pm \mu)$$

$$d\sigma \pm 2\sigma \tan \varphi \, d\theta - \frac{\gamma}{\cos \varphi}\left[\sin(\epsilon \pm \varphi)dx + \cos(\epsilon \pm \varphi)dz\right] = 0 \qquad (3)$$

where

c = cohesion

x,z = coordinates

γ = unit weight of soil

θ = angle between x axis and major principal stress

φ = angle of internal friction

ψ = c cot φ

μ = $\pi/4 - \varphi/2$

σ_1 = major principal stress (see Fig. 1)

σ_3 = minor principal stress (see Fig. 1)

σ = $(\sigma_1 + \sigma_3)/2 + \psi$

The equations are derived from the fundamental equations of plastic equilibrium and the Mohr-Coulomb failure criterion; this derivation may be found in detail elsewhere (Refs. 15,1). The coordinate system and notation for the specific problem of a driven rigid wheel are shown in Fig. 4. The shaded zones in the figure represent those areas in which the shear resistance of the soil has been fully mobilized and where failure is occurring. In Eqs. (3), the

upper sign refers to the family of slip lines corresponding to the first characteristics of the differential equations, the i-lines; the lower sign refers to the second characteristics, the j-lines. Figure 5 shows diagrammatically the orientation of the i and j characteristics (slip lines) and the indices used in computing values of x, z, σ, θ, and φ at the nodal point i,j.

As no closed form solution to these equations exists, numerical methods must be employed in which Eqs. (3) are replaced by four difference equations. An iterative scheme is used to obtain values for the desired variables at the point i,j from known values either previously computed at two adjacent points or specified at a boundary.

METHOD OF ANALYSIS

To compute the stress distribution at the soil-wheel interface and the slip line field in the soil beneath a driven rigid wheel, certain soil and wheel parameters must be specified. The soil parameters are: unit weight γ; the constants n, d, k, and c for Eq. (1) that provide the relationship between shear stress and normal stress on the failure envelope; and the friction parameter, δ. A relationship between δ and slip (i) proposed by Janosi and Hanamoto (Ref. 18) is used in this study with the modification that a constant for the threshold slip (i_o) at which movement starts, is included:

$$\tan \delta = \tan \varphi \left(e^{-(i+i_o)/K}\right) \tag{4}$$

where

i = slip

i_o = a constant to account for some threshold perimeter shear that may exist before wheel movement starts

K = an empirical constant.

The wheel parameters that must be specified prior to the computation are: the wheel radius (r_o) and width (b_o), and either the entry angle (α_e) or the rear angle (α_r) (Fig. 4) depending on whether the forward or rear field is being computed. For the analysis presented here, the separation angle (α_m) is assumed approximately equal to the angle δ. The literature contains some experimental and theoretical justification for this assumption (Refs. 16,17).

Within the computer program, there is provision for definition of additional geometric as well as stress boundary conditions. For example, the terrain may be made to slope at an angle ($\pm\epsilon$), and surcharge loadings (w) may be applied to the soil surface.

In the present analysis, a level surface essentially free of surcharge is assumed.

The method of analysis is based on a systematic application of the recurrence relationships implicit in Eqs. (3) to the wheel performance problem with its specific boundary condition. In this respect, it is similar to the method described in detail elsewhere for another problem (Ref. 19) with the added complication that an iteration procedure must be applied not only to σ_{ij} and θ_{ij}, but to φ_{ij} and ψ_{ij} as well. The following paragraph contains a brief description of the over-all computational procedure.

The rear field is computed first because experience has shown that for given wheel geometry and soil properties, the gradient of the stresses does not vary much with changes in α_r. This is a desirable feature in a trial-and-error solution procedure that requires matching the value of variables at a point common to two different computation sequences. The stress state and slip line field in the passive zone of the rear field are computed by Eqs. (3) starting at the surface for assumed values of α_r and L_r (see Fig. 4). In the radial shear zone, the same equations are used, but special consideration is given to the point where the j-lines converge. This point is a degenerated slip line, where θ changes from the value at the passive zone boundary to that specified at the active zone boundary. The total change in θ is divided by the number of slip lines converging at this point to obtain an equal $\Delta\theta$ increment between two adjacent slip lines. The σ value for each increment is computed from the equation $\sigma = \sigma_o \exp[2(\theta - \theta_o)\tan\varphi]$, which is the solution to Eqs. (3) if both dx and dz vanish. The same equations are used in the active zone except that for points along the soil-wheel interface, the values of θ are assigned. Along this boundary, the values

of δ and the wheel curvature must be considered in the specification of the θ values. The numerical computation is completed at i = h, j = k (see Fig. 5). At this point, the separation angle (α_m) is compared to δ. If the two values are within a specified tolerance of each other, the computation is continued to the forward zone. Otherwise, a new value is assumed for L_r and the stress state and slip line field computations are repeated for the rear field. This trial-and-error procedure is continued until the slip line field "closes" on the soil-wheel interface at an angle, α_m, approximately equal to $\delta_{h,k}$. In cases where closure cannot be obtained by varying L_r alone, α_r is also varied; however, the solution is not very sensitive to variations in α_r.

In the computation of the forward zone, the same basic procedure is followed: values of entry angle (α_e) and L_f are assumed and the passive (P), radial (R), and active (A) zone stress states and slip line fields are computed in that order (see Fig. 4). However, an additional criterion must be met for satisfactory "closure" of the forward field. Not only must the separation angle α_m equal $\delta_{h,k}$ as obtained from the rear field computation, but the magnitude and direction of the resultant stress at the point of juncture of the forward and rear fields must also be equal to that obtained from the rear field computations.

RESULTS

All results relate to an 8-inch-diameter, 2-inch-wide, rigid wheel being driven over medium dense (100 pcf), dry, Jones Beach sand. The failure criteria used in the analyses are determined from Fig. 2 and are expressed by Eq. (1) as follows:

$$\left(\frac{\tau}{1.0}\right)^{1.0} - \frac{\sigma_n}{1.1504} - 0 = 0 \qquad (\varphi = 41°) \tag{5}$$

$$\left(\frac{\tau}{1.0}\right)^{1.0} - \frac{\sigma_n}{1.3764} - 0 = 0 \qquad (\varphi = 36°) \tag{6}$$

$$\left(\frac{\tau}{1.0}\right)^{1.027} - \frac{\sigma_n}{1.1605} - 0 = 0 \qquad (\varphi \text{ - variable}) \tag{7}$$

where τ and σ_n are in units of pounds per square foot.

Values of friction parameter ($\delta = 15°$, $\delta = 21°$, and $\delta = 25°$) were combined with the internal friction angles considered to yield a range of slips from 18 to 52 percent. Slips were calculated from δ and φ by Eq. (4) with empirically determined values of the constants K and i_o.

All computations were performed in real time on an On-Line Systems computer based on Digital Equipment Corporation's PDP-10 processors. After the computation of their coordinates, slip line fields and stress distributions were plotted in a matter of seconds on an Adage Inc. visual display CRT via a graphics terminal connected with the computing system. This interaction between the graphics and computing systems allowed almost immediate viewing of the results to ascertain that no irregularities existed in the solution, and to acquire a visual perception of the interrelationship among the many parameters.

Slip Line Fields and Stress Distributions

Figure 6 shows the slip line fields for the upper- and lower-boundary straight-line failure envelopes for Jones Beach sand ($\varphi = 36°$ and $\varphi = 41°$) and for the nonlinear (φ - variable) envelope. The results are for a soil-wheel interface friction of 15 degrees. For comparison, a rear angle of 5 degrees was chosen. It is clear from Fig. 6 that the entry angle (α_r) in each case is about the same and equal to approximately 22 degrees. Therefore, the sinkage given by $S = r_o (1 - \cos \alpha_r)$ is also approximately the same in each case (0.3 in.). What is clearly different is the geometric extent of the slip line field; it is the largest for $\varphi = 41$ degrees and about the same for $\varphi = 36$ degrees and φ - variable. This means that in the former case, more soil material is affected and more frictional resistance is mobilized than for the other two cases. Consequently, the vertical load that the wheel can carry is greater for $\varphi = 41$ degrees than for the other two cases. A summary of the performance characteristics of the wheel for the three cases is given in Table 1. It can be seen

Table 1

SUMMARY OF PERFORMANCE CHARACTERISTICS
FOR DRIVEN RIGID WHEEL ON JONES BEACH SAND

φ (deg)	δ (deg)	α_r (deg)	L_r	α_f (deg)	L_f	S (in.)	W (lbs)	DB (lbs)	T (ft-lbs)
41	15	5	12	23.1	2	0.32	9.81	0.61	0.85
36	15	5	8.2	22.0	1.4	0.29	3.96	0.29	0.34
Var.	15	5	9.4	22.0	1.6	0.29	5.34	0.41	0.47

from this table that although the extent of slip line fields for φ = 36 degrees and φ - variable looks about the same, the wheel performance characteristics in each case are quite different. That the values of load, drawbar, and torque are greater for φ - variable than for φ = 36 degrees is directly attributable to the fact that at points within the slip line field where stresses are relatively low, φ in the former case is larger than 36 degrees. Consequently, at those points more volume is affected and more frictional resistance is mobilized than would be the case for φ = 36 degrees. This occurs mainly along the free surface boundaries and within the active zones so that the active zones for φ - variable are slightly larger than those of φ = 36 degrees. Because the curvature of the failure envelope of Jones Beach sand is not extreme, this difference is rather small and cannot be easily noticed in Fig. 6. However, a comparison of L values in Table 1 shows that the effect is real and does indeed exist. From Fig. 6, it is seen that along with the soil-wheel interface, the passive zones in each case are almost identical. This is expected since the stresses within those zones are at a level where φ - variable is almost equal to 36 degrees.

Figures 7, 8, and 9 represent the normal and shear stress distributions along the soil-wheel interface that correspond to the three slip line fields shown in Fig. 6. The shape of the distributions is characteristic of that determined experimentally for a driven wheel by us and Sela in Ref. 16. The maximum normal and shear stresses occur as specified at an angle (α_m) equal to δ (see Fig. 4). The integration of the vertical and horizontal components of the normal and shear stress over the contact area yields, respectively, the values for load and drawbar given in Table 1. The torque is determined directly from the shear stress distribution.

The nature of the lateral distribution has not yet been defined analytically so that at present we assume the normal and shear stress distributions to be uniform over the width of the wheel even though we know from experiments that this is not always the case.

Performance Characteristics As a Function of Sinkage and the Slip-Sinkage Relationship

The effect of variable φ on the performance characteristics of the wheel under study is shown in Figs. 10, 11, and 12. In these illustrations, load, drawbar, and torque are plotted as a function of sinkage for the three failure envelopes considered at a δ of 15 degrees. The illustrations show that in all cases the results of the φ - variable analysis lie between the other two and seem to give an "average" curve. Closer inspection shows that this is not the case. At low sinkage (a situation that occurs at relatively low over-all stress levels), the φ - variable curve is much closer to the $\varphi = 41$ degree curve. This is expected because at low stress levels the φ - variable strength envelope approaches the $\varphi = 41$ degree Mohr-Coulomb curve. To use an "average" curve would result in somewhat lower load and drawbar, and higher torque than predicted by the φ - variable analysis. The differences are small for the case in point; however, for a material with an extremely curved failure envelope the differences would be magnified, and use of either the $\varphi = 41$ or $\varphi = 36$ degrees failure envelope exclusively would introduce significant errors in the computation of performance parameters.

Figure 13 shows the slip-sinkage relationship derived from Eq. (4) for Jones Beach sand, and the results of the nonlinear failure envelope analysis. From top to bottom, the three curves

shown correspond to interface friction (δ) values of 25°, 21°, and 15°, respectively. Since δ and the normal and shear stresses acting along the soil-wheel interface are related (refer to Fig. 3), it is clear that slip-sinkage relationships of the form shown in Fig. 13 are actually an expression of soil-wheel interaction and its effect on the magnitude and direction of the normal and shear stress distributions.

Relationship of Performance Coefficients to Slip for Jones Beach Sand

In the prediction of tire performance, it is customary to plot experimentally determined performance coefficients versus a dimensionless number called the mobility number. For sand, the mobility number is a function of the cone index gradient, vertical load, and loaded and unloaded tire geometry (Ref. 20). Because the mobility number is zero when there is no wheel deflection, this term cannot be used as a predictive parameter for rigid wheels. Consequently, for this study on Jones Beach sand, two performance coefficients, the pull coefficient (drawbar/vertical load) and the torque coefficient [torque/(vertical load × wheel radius)] are plotted in Fig. 14 versus another dimensionless parameter, slip. In the computation of load, torque, and drawbar, a nonlinear failure envelope was used. The plot differs from the conventional pull or torque versus slip plot (see e.g., Ref. 21) in that it contains no pronounced curvature with increasing slip that would correspond to a maximum pull point or a maximum torque level. However, the portion of the plot about the origin can still be used to determine the "self-propelled" point (value of slip at $DB/W = 0$) and/or the "towed point" (the value of slip and DB/W at $T/Wr_o = 0$).

The results of two preliminary tests (Test Nos. 090101 and 090102) run with an 8-inch-diameter, 2-inch-wide wheel on Jones Beach sand in the mobility test bin at Grumman are also plotted in Fig. 14. The points are seen to be quite close to the theoretically derived predictive curves for the same material.

SUMMARY AND CONCLUSIONS

A theory of soil-wheel interaction based on plasticity theory and a general representation of the Mohr yield criterion has been developed. Computer solutions of the differential equations of equilibrium are used to obtain the slip line fields and associated interface stresses for a specific wheel geometry and three different representations (two linear, one nonlinear) of the Mohr failure envelope of the supporting soil material. Load, drawbar pull, and torque are calculated from the computed interface stresses and are compared for the three failure envelopes. For each of these performance parameters, the values for a given sinkage obtained with the nonlinear failure envelope lie between those obtained with the upper- and lower-boundary straight-line approximations.

With the use of the newly developed theory, numerical computations are performed that clearly show the effect of interface friction on the relationship between slip and sinkage. Prediction relationships for pull and torque coefficients are developed as a function of slip. Experimental results are shown to compare favorably with the analytically derived prediction relationships.

The results of this analysis suggest that for those soils where the Mohr failure envelope is significantly curved (some partially saturated soils and certain types of overconsolidated clays), the use of straight-line approximations or "average" envelopes may introduce considerable error in the computation of mobility performance parameters.

ACKNOWLEDGMENT

The authors wish to acknowledge the contribution of Mr. George Homfeld of Grumman Aerospace Corporation in the performance of the experimental portions of this research.

REFERENCES

1. Sokolovskii, V., Statics of Granular Media, Pergamon Press, New York, 1965.

2. Graham, J., "Plane Plastic Failure in Cohesionless Soils," Geotechnique, Vol. XVIII, No. 3, 1968, pp. 301-316.

3. Kurtay, T. and Reece, A., "Plasticity Theory and Critical State Soil Mechanics," Journal of Terramechanics, Vol. 7, Nos. 3-4, 1970, pp. 23-56.

4. Karafiath, L., "On the Effect of Pore Pressures on Soil-Wheel Interaction," Proceedings Fourth International Conference on the Mechanics of Soil Vehicle Systems, Stockholm, Vol. I, 1972.

5. Nowatzki, E., "A Theoretical Assessment of the SPT," Proceedings, Fourth Pan-American Conference on Soil Mechanics and Foundation Engineering, Vol. II, 1971, pp. 45-61.

6. Hill, R., The Mathematical Theory of Plasticity, Clarendon Press, Oxford, 1950.

7. Szymanski, D., "Some Plane Problems of the Theory of Limiting Equilibrium of Loose and Cohesive, Nonhomogeneous Isotropic Media in the Case of a Nonlinear Limit Curve," in Nonhomogeneity in Elasticity and Plasticity (ed. by W. Olszak), Pergamon Press, New York, 1958

8. Kingston, M. and Spencer, A., "General Yield Conditions in Plane Deformations of Granular Media," Journal of the Mechanics and Physics of Solids, Vol. 18, 1970, pp. 233-243.

9. Jo-Yung Wong, J. and Reece, A., "Soil Failure Beneath Rigid Wheels," Proceedings Second Intl. Conf. of the Intl. Soc. for Terrain Vehicle Systems, University of Toronto Press, 1966.

10. Wiendieck, K., Contribution to the Mechanics of Rigid Wheels on Sand, U.S. Army Engineer Waterways Experiment Station, Technical Report M-68-2, May 1968.

11. Hettiaratchi, D. and Reece, A., "Symmetrical Three Dimensional Soil Failure," Journal of Terramechanics, Vol. 4, No. 3, 1967, pp. 45-67.

12. Vincent, E., "Pressure Distribution on and Flow of Sand Past a Rigid Wheel," Proceedings First International Conference on the Mechanics of Soil Vehicle Systems, Torino, 1961, pp. 858-78.

13. Terzaghi, K., Theoretical Soil Mechanics, John Wiley and Sons, Inc., New York, 1943.

14. Karafiath, L., "Analysis of Stress Distribution beneath Wheels by the Theory of Plasticity with Respect to Lunar Locomotion," Proceedings ISTVS-TRW Off-Road Mobility Symposium, 1970, pp. 49-76.

15. Harr, M., Foundations of Theoretical Soil Mechanics, McGraw-Hill Book Company, New York, 1966.

16. Sela, A., The Shear to Normal Stress Relationship between a Rigid Wheel and Dry Sand, USATAC, Land Locomotion Laboratory Report RR8524, 1964.

17. Karafiath, L., "Plasticity Theory and the Stress Distribution beneath Wheels," Journal of Terramechanics, Vol. 8, No. 2, 1971, pp. 49-60.

18. Janosi, Z. and Hanamoto, B., "The Analytical Determination of Drawbar Pull As a Function of Slip for Tracked Vehicles in Deformable Soils," Proceedings First International Conference on the Mechanics of Soil Vehicle Systems, Torino, 1961, pp. 707-727.

19. Nowatzki, E. and Karafiath, L., "The Effect of Cone Angle on Penetration Resistance," Highway Research Record (in press).

20. Freitag, D., A Dimensional Analysis of the Performance of Pneumatic Tires on Soft Soils, Technical Report No. 3-688, U.S. Army Engineer Waterways Experiment Station, CE, Vicksburg, Mississippi, 1965.

21. Turnage, G., "Tire Selection and Performance Prediction for Off-Road Wheeled-Vehicle Operations," Proceedings Fourth International Conference on the Mechanics of Soil Vehicle Systems, Stockholm, Vol. I, 1972, pp. 61-82.

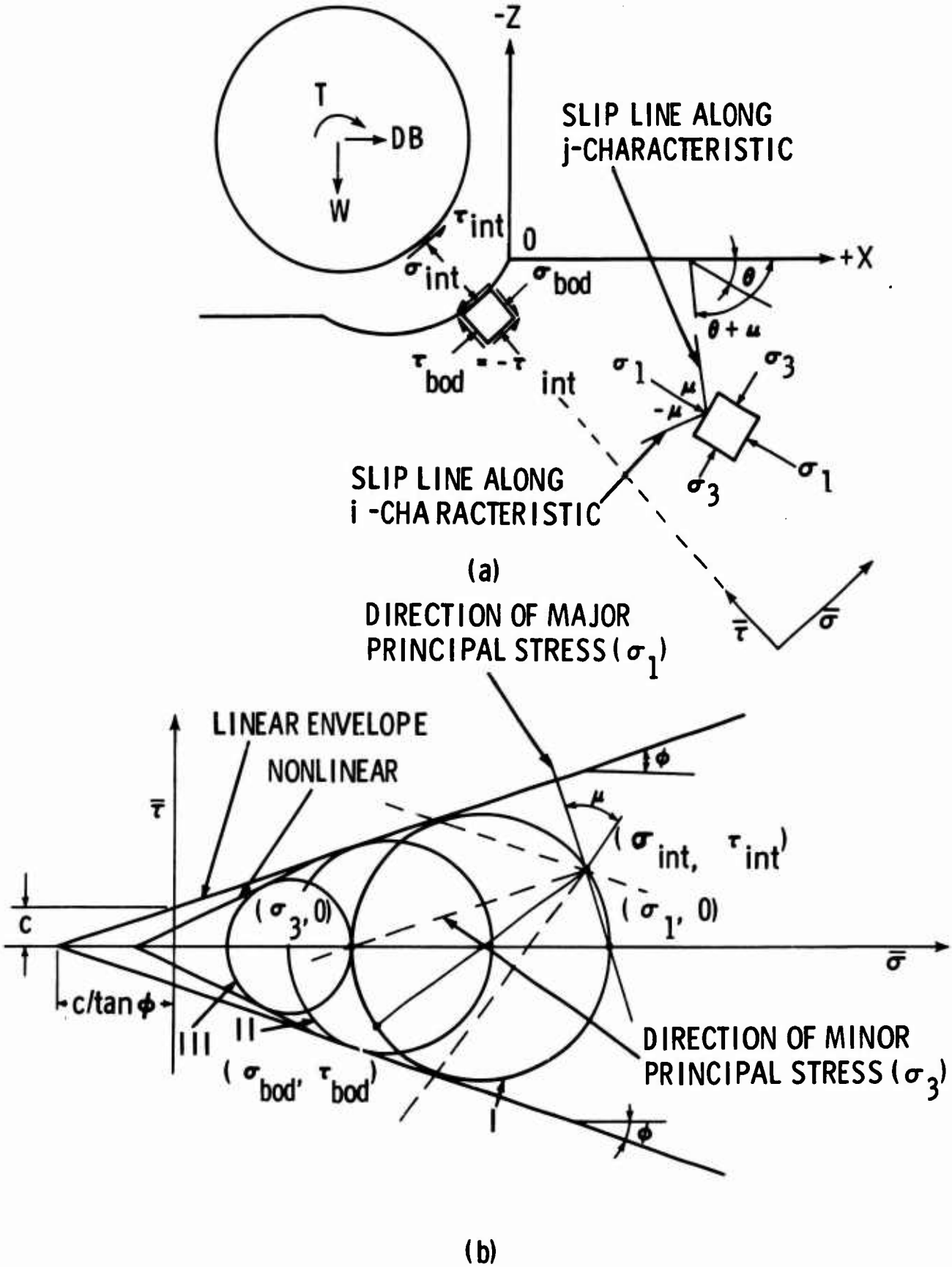

Fig. 1 Mohr Circle Representation of Interface Stresses

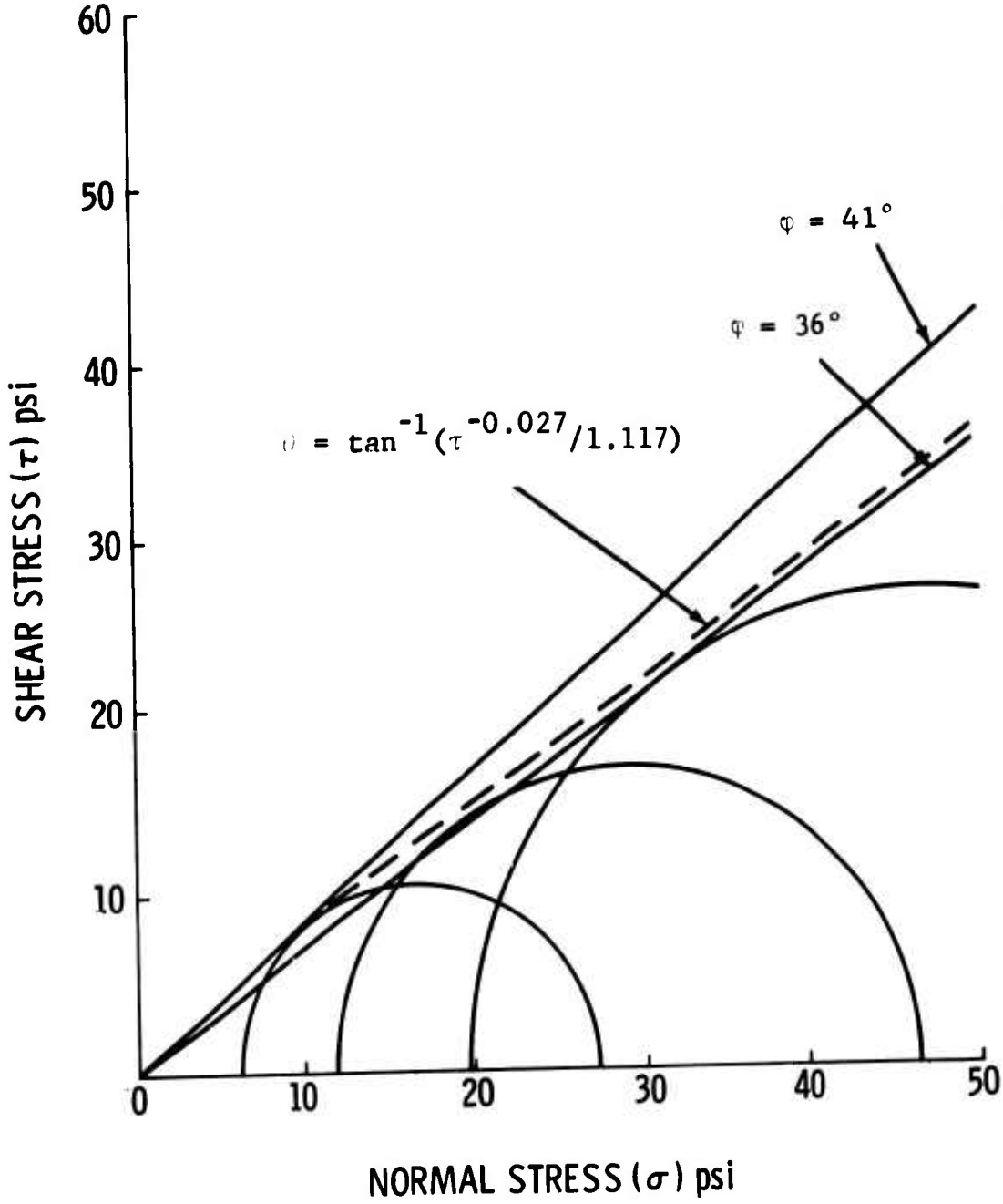

Fig. 2 Mohr Diagram — Result of Triaxial Tests on Jones Beach Sand

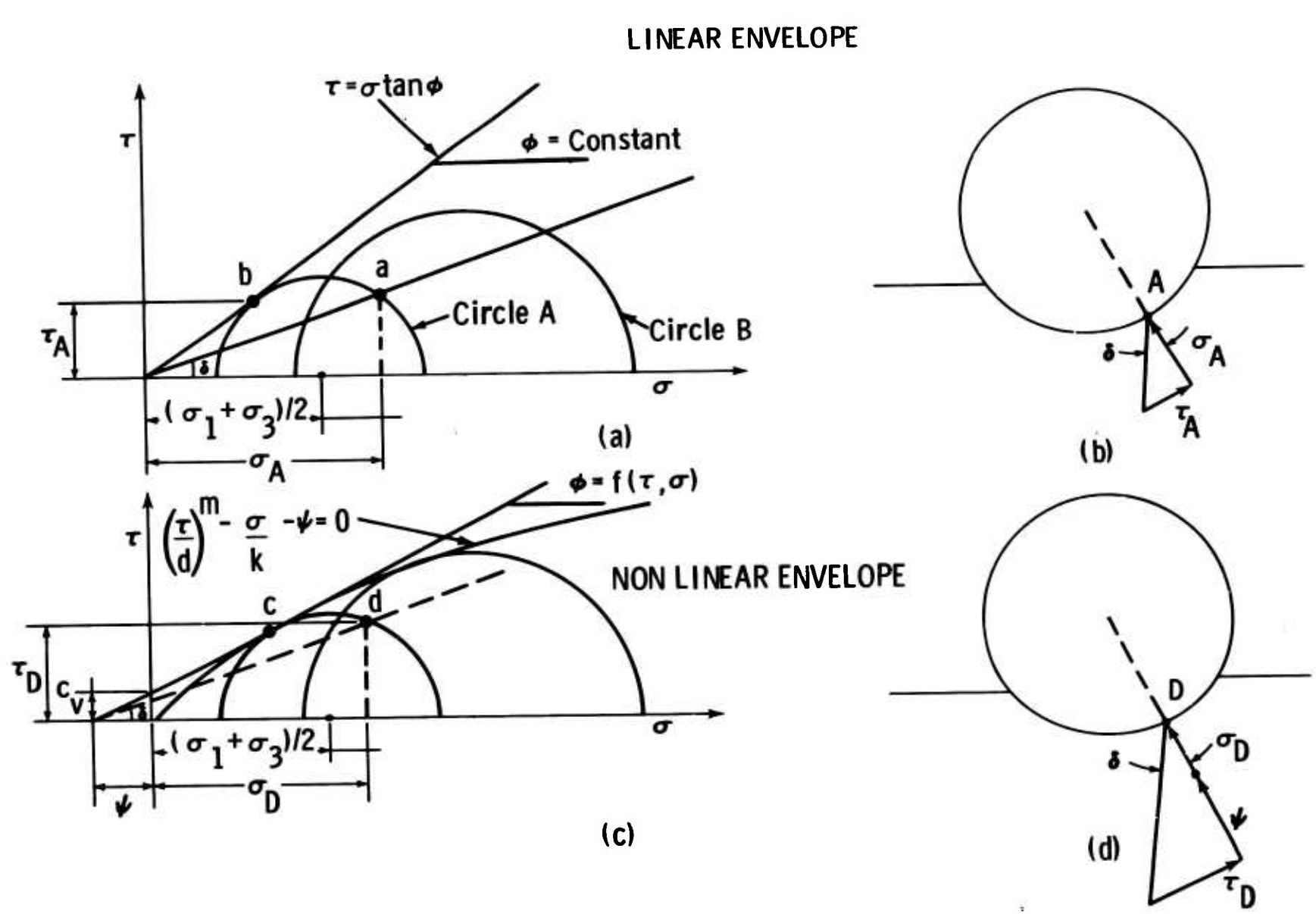

Fig. 3 The Effect of a Nonlinear Mohr Failure Envelope on the Magnitude and Nature of Interface Stresses

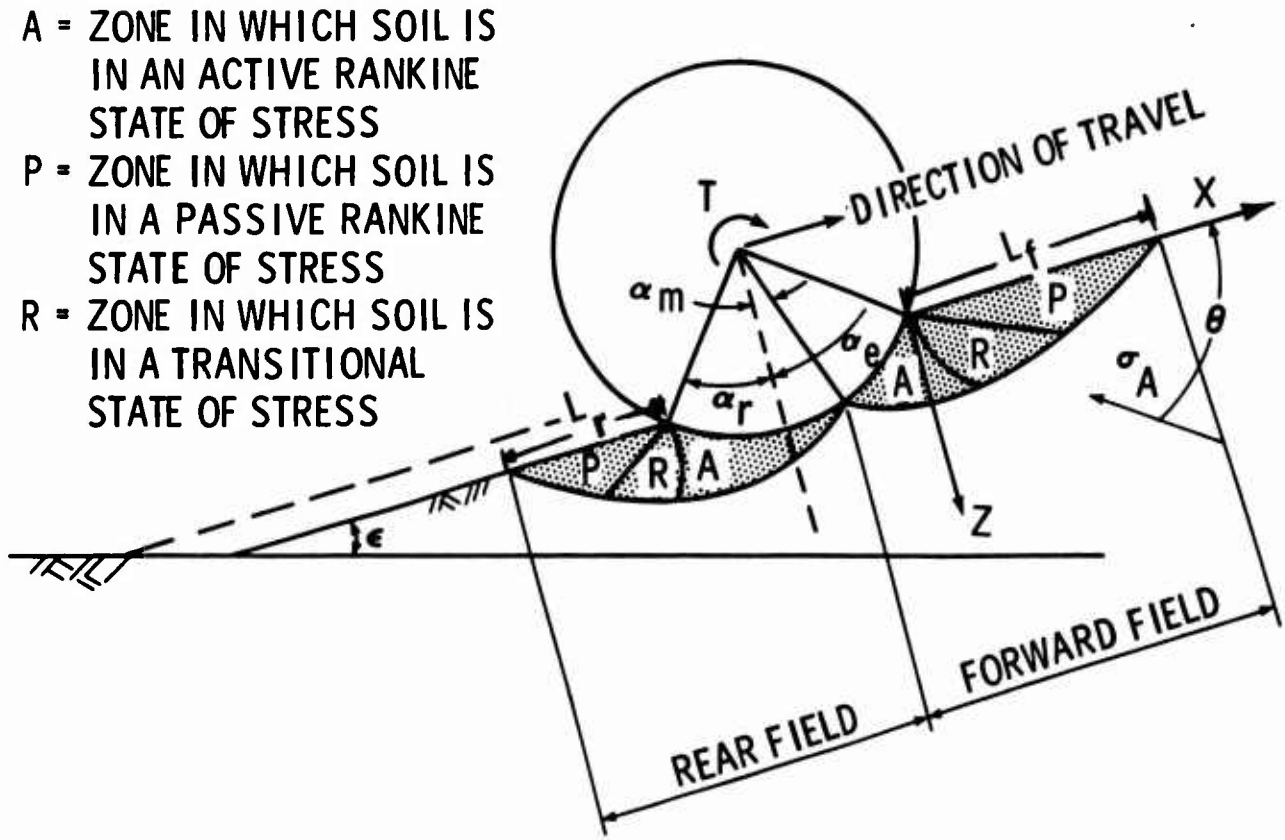

Fig. 4 Definition of Problem Geometry

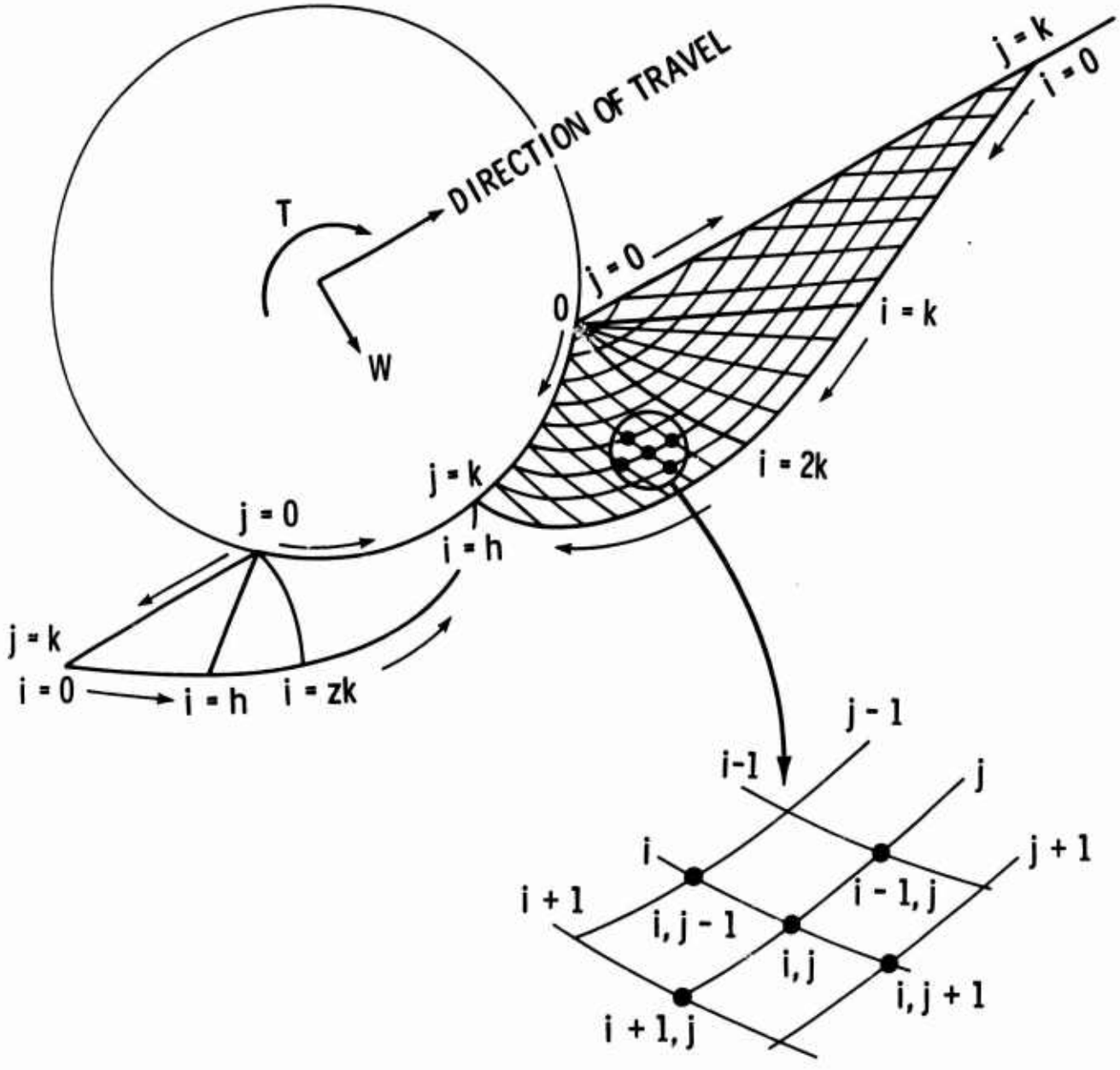

Fig. 5 Diagram of Indexing Scheme Used in Numerical Solution of Equilibrium Equations (Arrows along Boundaries Indicate Direction of Increasing i- and j-Indices)

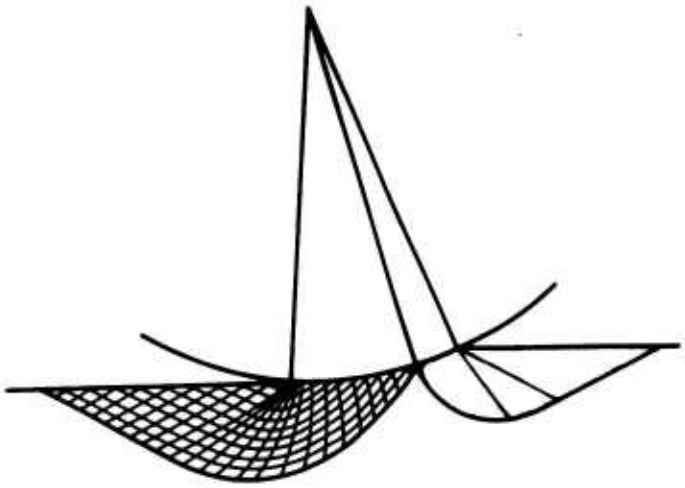

(a) PHI = 36

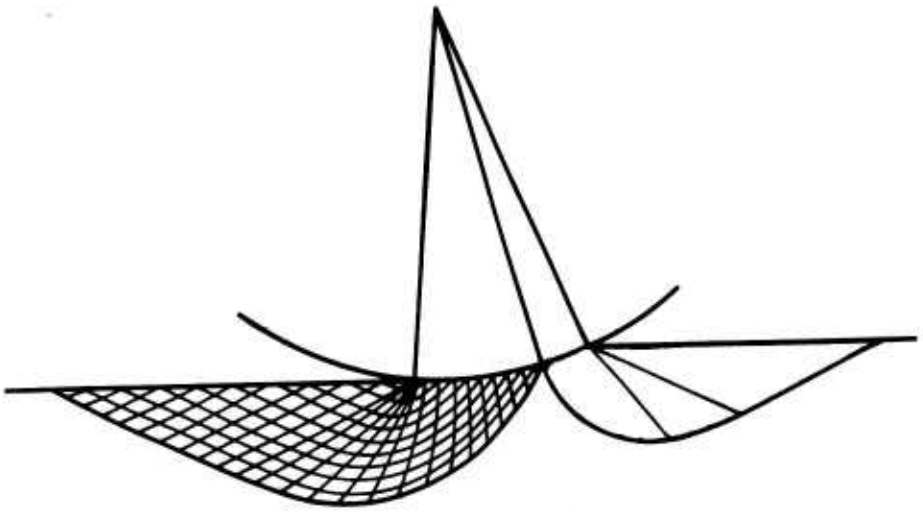

(b) PHI = 41

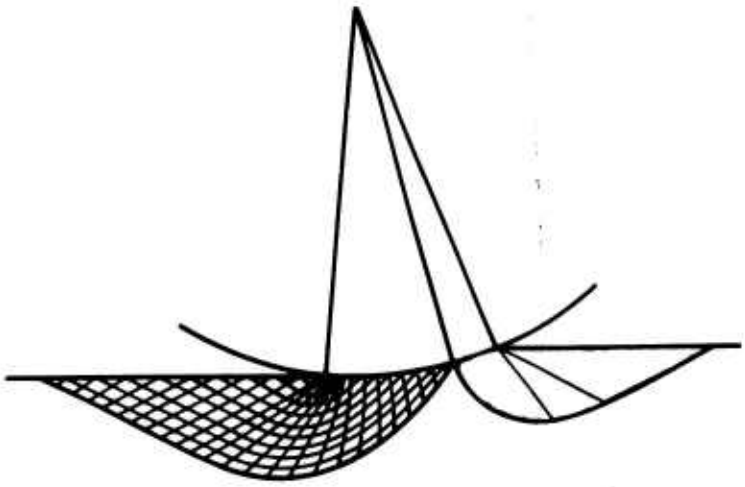

(c) PHI = VAR

Fig. 6 Variation of Slip Line Field with Friction Angle (δ = 15°)

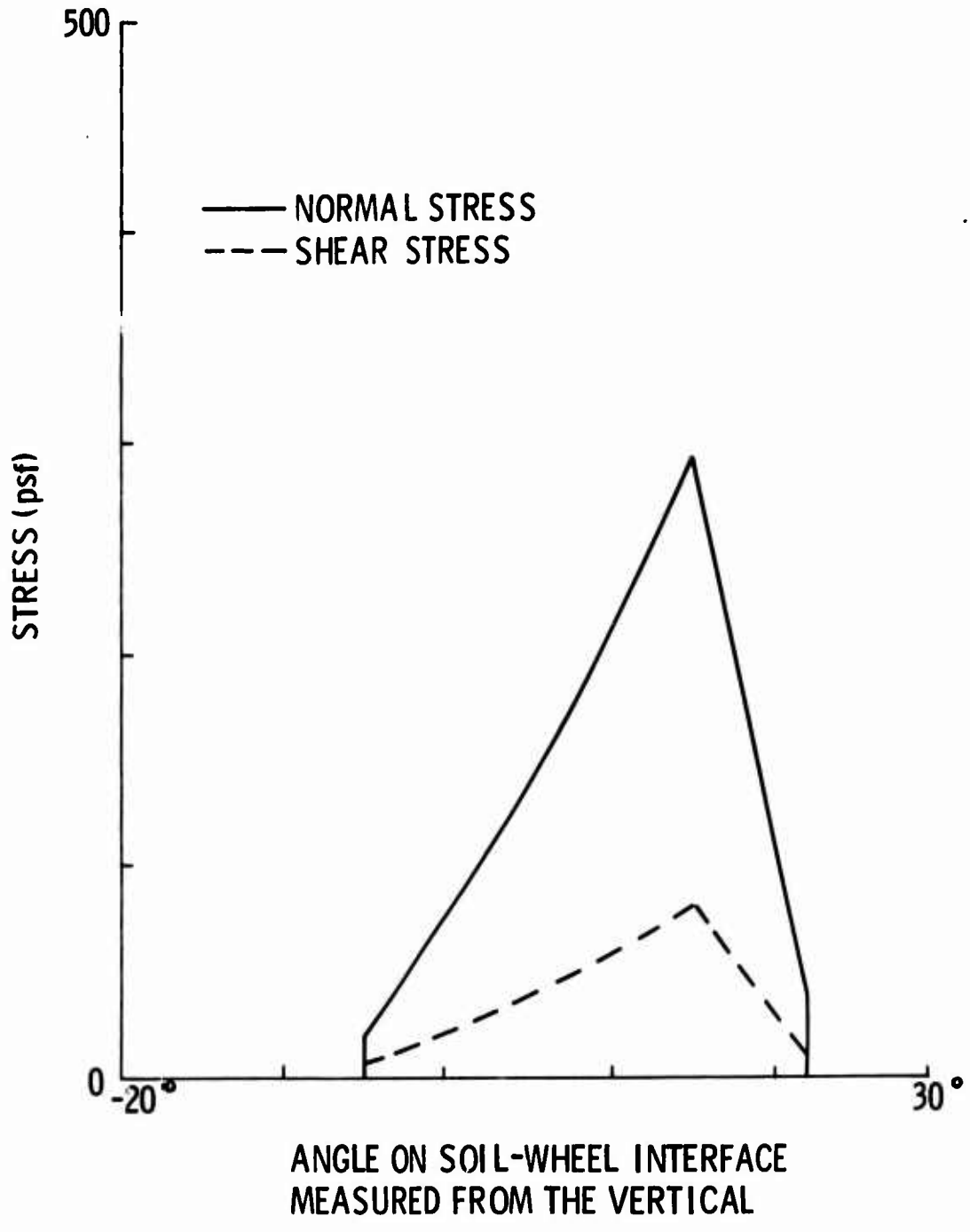

Fig. 7 Interface Stresses: $\Phi = 36°$, $\delta = 15°$

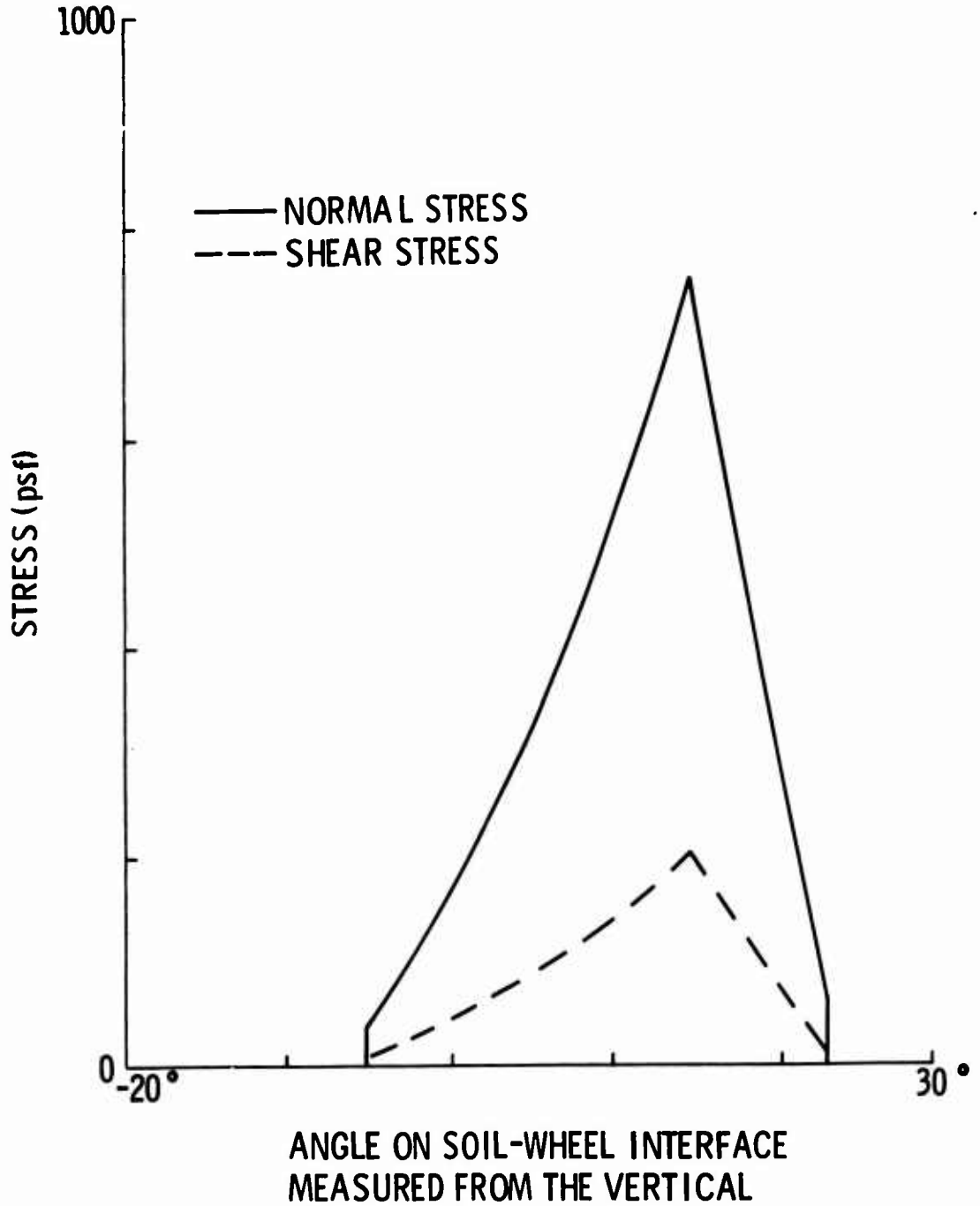

Fig. 8 Interface Stresses: $\varphi = 41°$, $\delta = 15°$

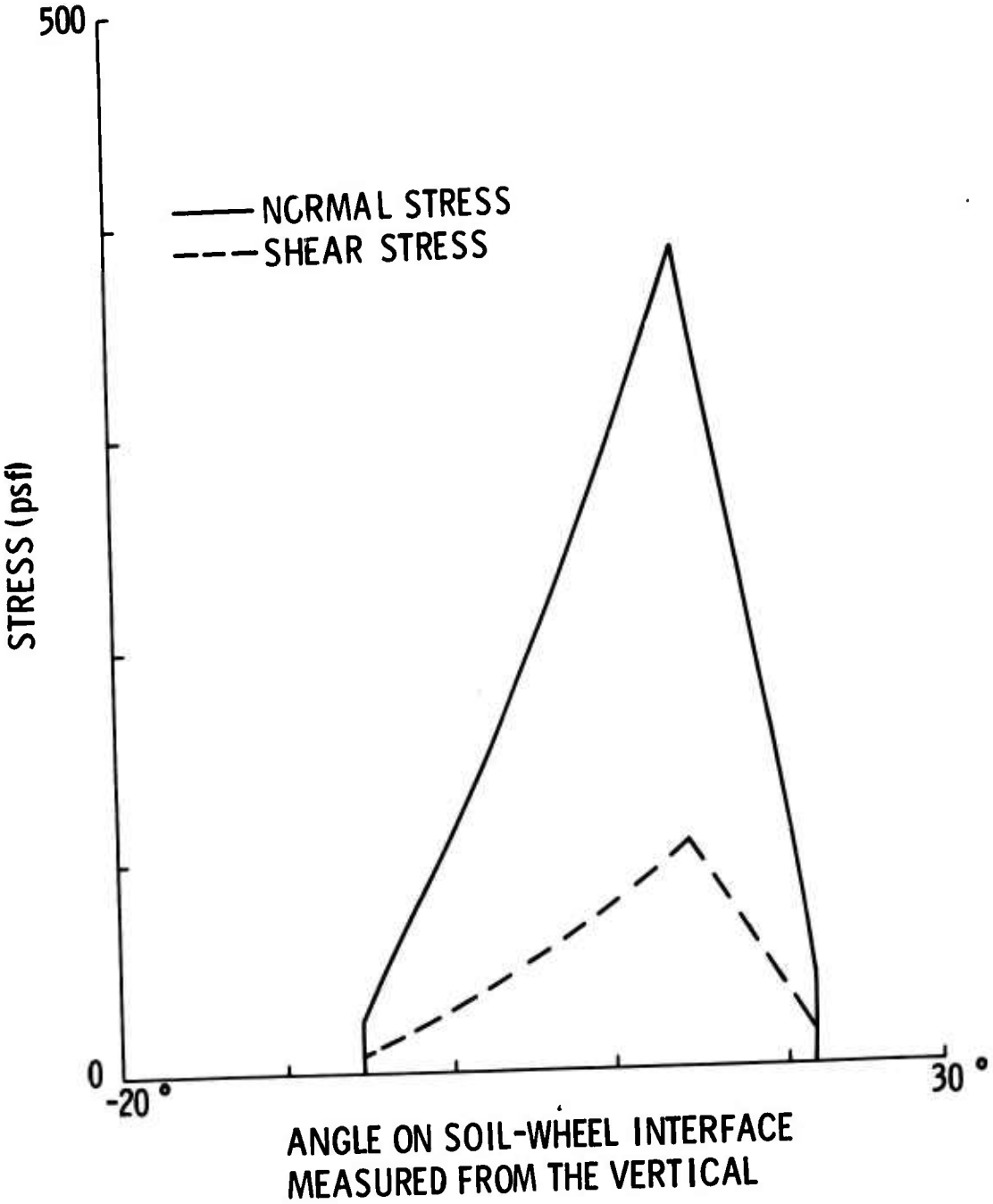

Fig. 9 Interface Stresses: φ = Variable, δ = 15°

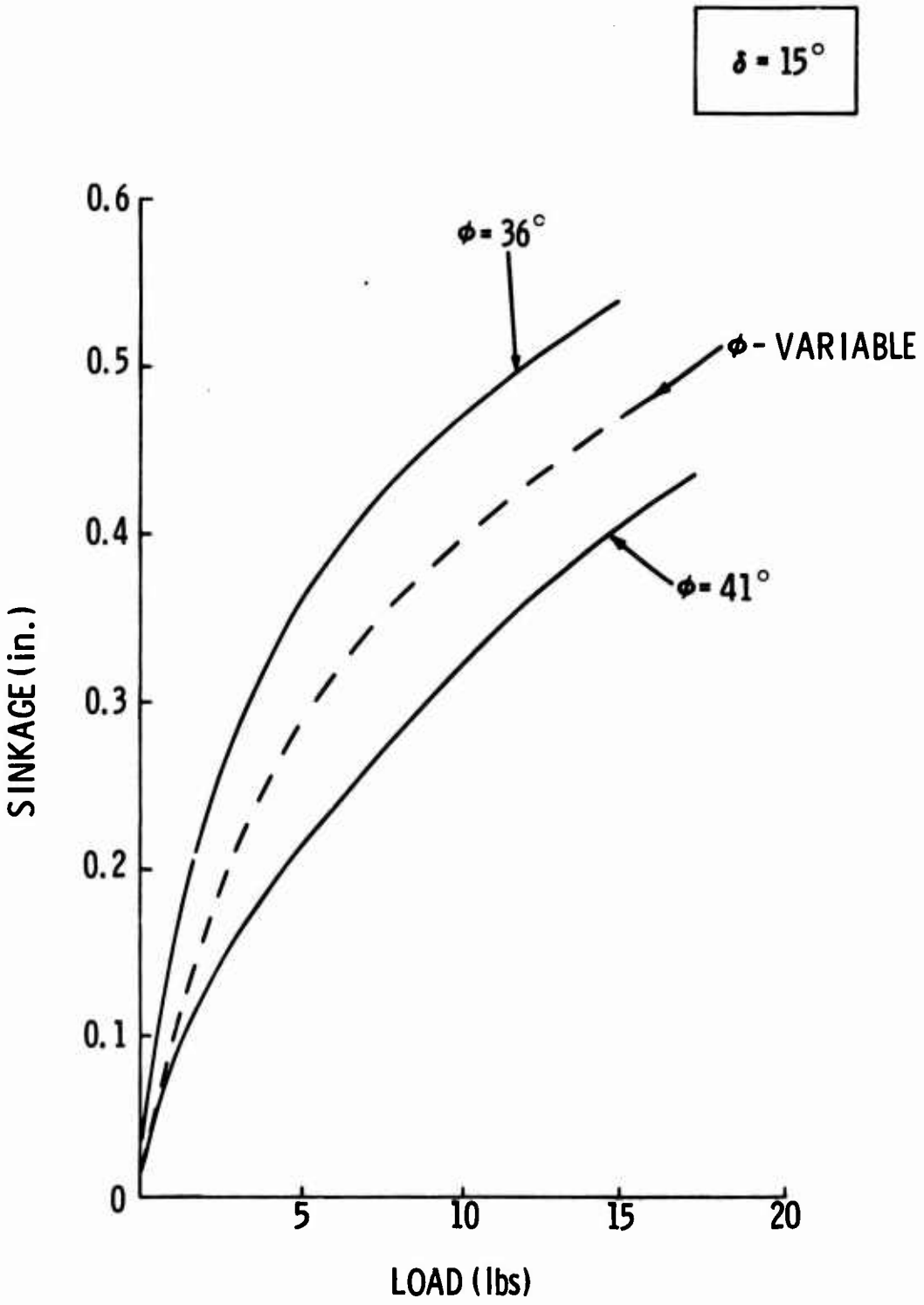

Fig. 10 Load-Sinkage Relationship for 8-Inch-Diameter, 2-Inch-Wide Rigid Wheel Driven on Jones Beach Sand

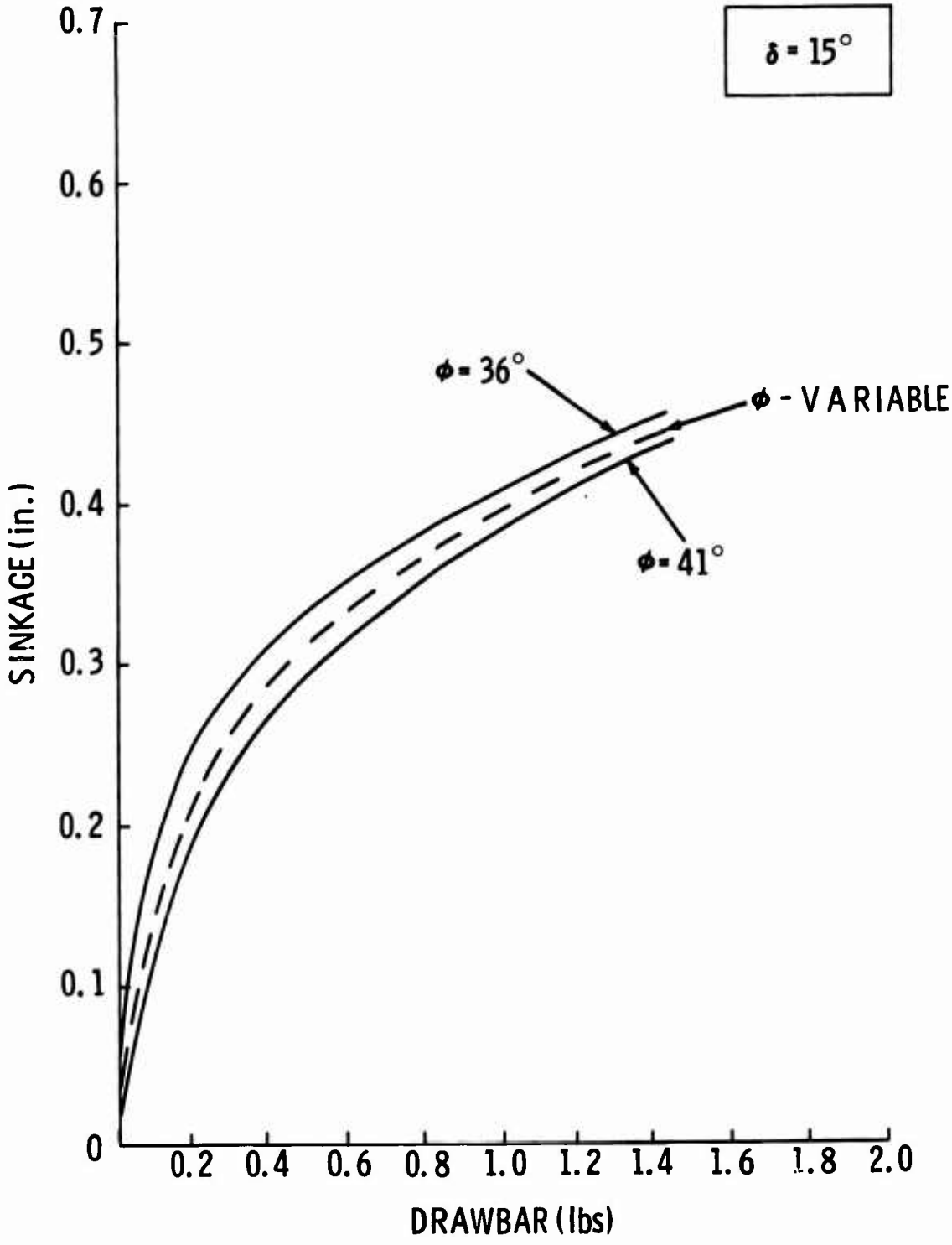

Fig. 11 Drawbar Pull (Drag) – Sinkage Relationship for 8-Inch-Diameter, 2-Inch-Wide Rigid Wheel Driven on Jones Beach Sand

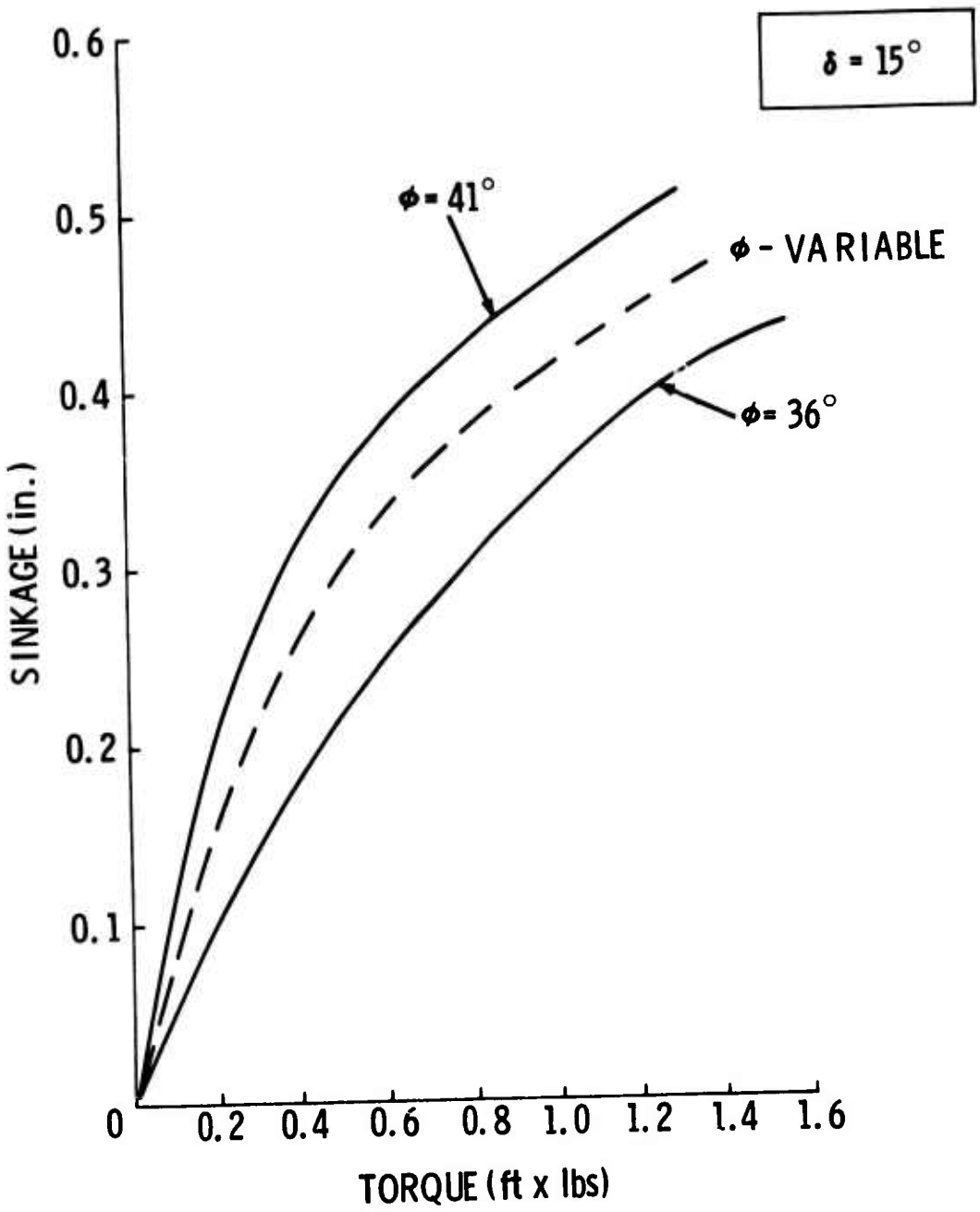

Fig. 12 Torque-Sinkage Relationship for 8-Inch-Diameter, 2-Inch-Wide Rigid Wheel Driven on Jones Beach Sand

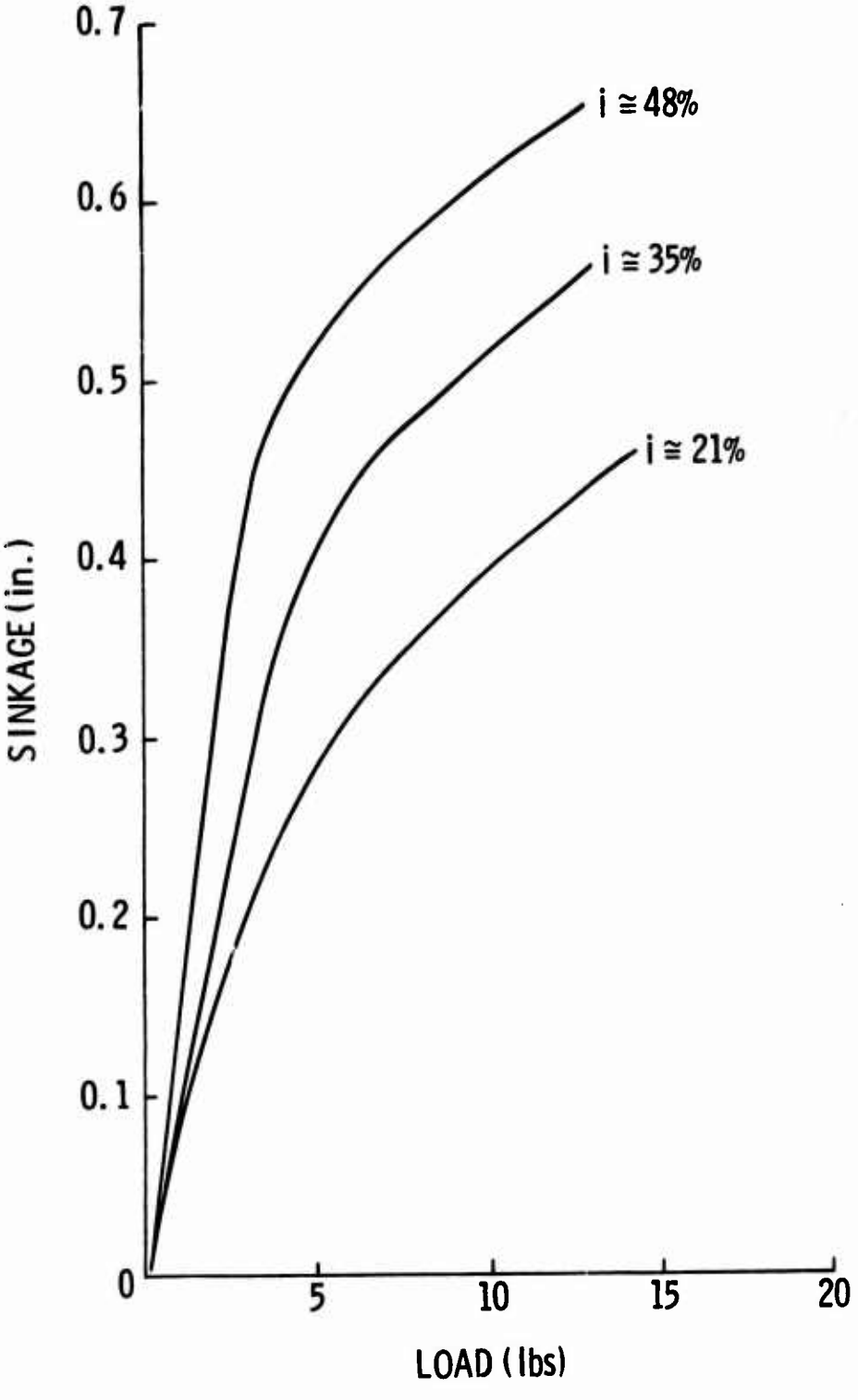

Fig. 13 Slip-Sinkage Relationship for 8-Inch-Diameter, 2-Inch-Wide Driven Rigid Wheel on Jones Beach Sand

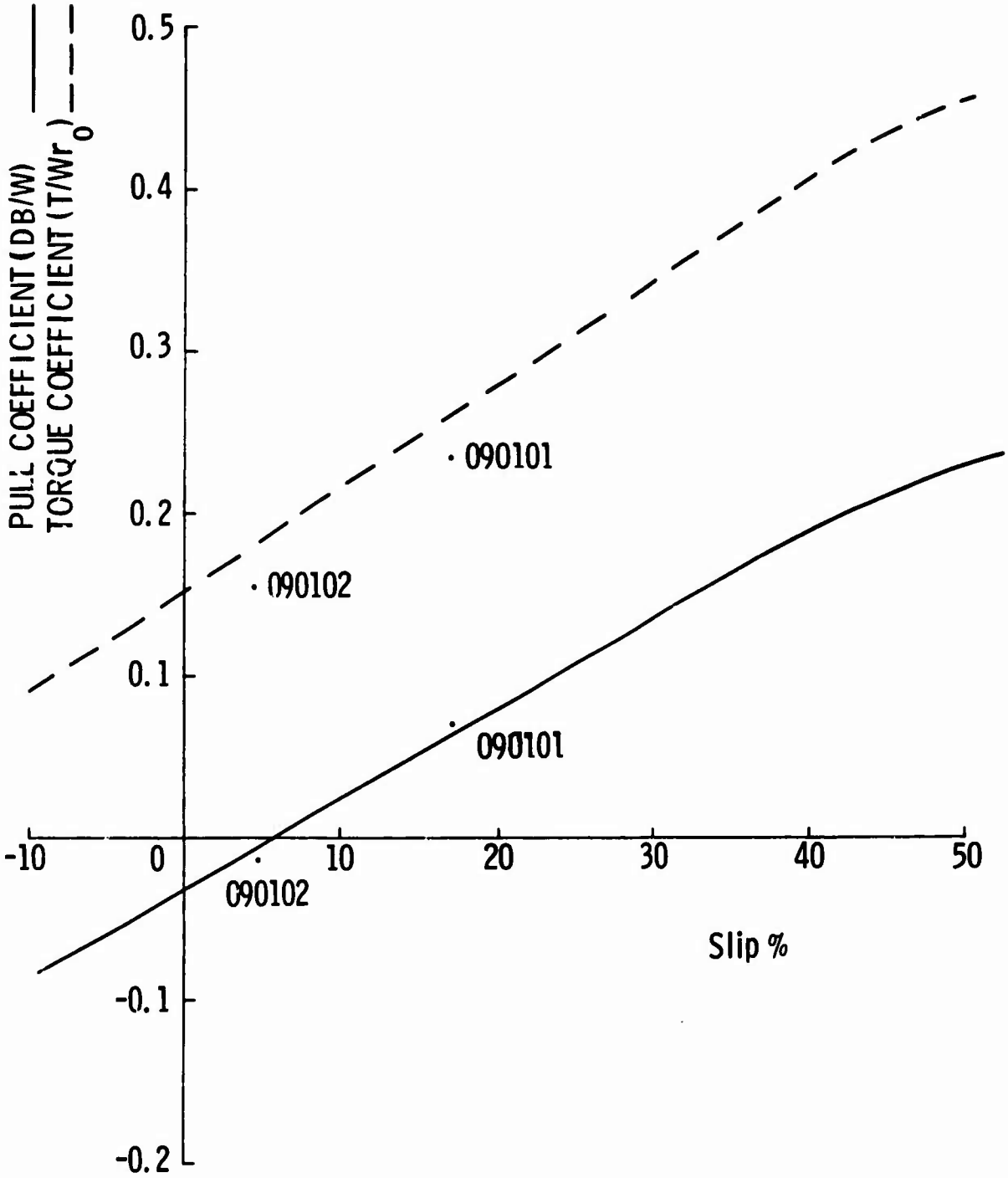

Fig. 14 Relationship of Performance Coefficients to Slip for Jones Beach Sand